Received: 23 January 2022 | Revised: 28 July 2022 | Accepted: 14 September 2022

DOI: 10.1002/mmce.23438

ORIGINAL ARTICLE

INTERNATIONAL JOURNAL OF RF AND MICROWAVE COMPUTER-AIDED ENGINEERING WILEY

Sharp roll-off triband microstrip bandpass filter with wide stopband for multiband wireless communication systems

Muhammad Riaz | **Bal S. Virdee** | **Dion Mariyanayagam** | **Shahram Salekzamankhani** | **Harry Benetatos** | **Innocent Lubangakene**

Center of Communications Technology, School of Computing and Digital Media, London Metropolitan University, London, UK

Correspondence
Bal S. Virdee, Center of Communications Technology, School of Computing and Digital Media, London Metropolitan University, London, UK.
Email: b.virdee@londonmet.ac.uk

Abstract

Design of a novel triband bandpass filter is presented for wireless communications systems. The filter is based on inter-coupled stepped impedance resonators and inter-digitally coupled to the input/output ports. The configuration of the filter circuit consists of open-loop resonators that are electromagnetically coupled to each other using inverted T-shaped open stubs. The intrinsic characteristics of filter structure generates five transmission zeros that results in triband bandpass response exhibiting sharp selectivity, high inter-band isolation and a wide out of band rejection. Unlike other triband filters reported recently in literature the proposed single layer filter does not require any short-circuited plated through hole which can introduce fabrication complexity and therefore production costs. Moreover, the triband structure can be configured to provide passbands with identical 3-dB fractional bandwidth and whose center frequency can be equally spaced. In the proposed prototype design presented here the passband frequencies are set to 3.6, 4.6, and 5.6 GHz that corresponds to WiMAX, 5G, and WLAN applications. The consequence of employing open-circuited transmission lines in the design results in a relatively large structure, which can be overcome by employing higher dielectric constant substrate. The proposed triband filter was designed to achieve identical 3-dB fractional bandwidth of 11.9%. Measured results confirm inter-band isolation better than 30-dB. The theoretical model is consistent with the measured results.

KEYWORDS

bandpass filter, inter-digitally coupled feedlines, microstrip, stepped impedance transmission-lines, wideband

1 | INTRODUCTION

PLANAR multiband microwave filters with characteristics of low-loss, sharp selectivity, compact size, and high inter-band solation are in high demand for modern and emerging multi-mode wireless communication systems that need to accommodate different communications standards. Multiband filters are vital components that address the challenges of isolating closely spaced adjacent communications channels in a highly congested electromagnetic spectrum. Good isolation and wide stopband are needed to reject interferences from other wireless systems in the multiband. The design of multiband microwave filters is more challenging as compared to dual band filters in terms of compactness and performance. This is because of the closely spaced passbands in commercial wireless systems, for example, GSM, Wi-Fi and WiMAX systems operate at 3.5, 5.2/5.25, 0.9/1.8, and 2.4/2.45 GHz bands, respectively.[1] Numerous examples of multiband bandpass filters have been recently reported exploiting the multiple mode behavior of stepped impedance resonators, short or open stub loaded resonators and dual mode loop resonators.[2–7] In Reference [8], the multiband filter design using a stub loaded stepped impedance resonator (SIR) is implemented with defected microstrip structure. In Reference [9], the resonant modes of stub loaded resonators are controlled by varying the length of center-loaded stub. A triband bandpass filter with stubs loaded stepped impedance resonator is proposed in Reference [10], where the frequency of the first three resonant modes is influenced by the short and open stubs and shorted high impedance section of stepped impedance resonator. Although the performance of the above multiband filters exhibit acceptable passband selectivity and generally acceptable band-to-band isolation however the filters require short circuited vias or use complex cross-coupling structures to generate multiple transmission zeros. Moreover, the 3-dB bandwidth of their passbands is uncontrollable.

In this paper, a novel frequency discriminating microstrip based structure is presented that exhibits triband filtering characteristics for wireless multiband communication systems. The proposed bandpass filter can be implemented on a single layer of standard dielectric substrate, and it was designed to extract GSM, Wi-Fi and WiMAX signals. The bandpass filter is based on stub-loaded half-wavelength resonators that are electromagnetically coupled to each other and the input/output ports. Inter-digitally coupled feedlines are used to realize a wide stopband with high attenuation on the upper and lower sides of the filter response. The filter structure creates triband responses by exciting multiple transmission zeros. Unlike other multiband filters, the proposed multiband filter is of a novel configuration that can be implemented/printed on a single layer of substrate and does not require any metallic vias. The triband filter exhibits desirable characteristics of highly sharp selectivity (>119 dB/GHz), parity 3-dB fractional bandwidth (11.9%), excellent inter-band isolation (>30 dB), passband insertion-loss (0.78 dB), and a wide stopband performance. These characteristics are analogous to filters based on high-temperature superconductors (HTS), but unlike HTS devices the proposed filter does not require cryogenic cooling.[11] The performance of the filter was validated through measurement.

2 | GEOMETRY OF THE PROPOSED TRI-BAND BANDPASS FILTER

Configuration of the proposed quasi-elliptic triband bandpass filter is shown in Figure 1. The filter consists of U-shaped open-loop resonators of half-wavelength long that are electromagnetically coupled to each other via T-shaped resonators, and inter-digitally coupled to the input/output ports. The open-loop resonators include stepped impedance sections. This structure can be characterized as having periodicity of two.

Total admittance of the microstrip resonator coupled with the input/output feedline and the T-shaped resonator, shown in Figure 2, is given by:

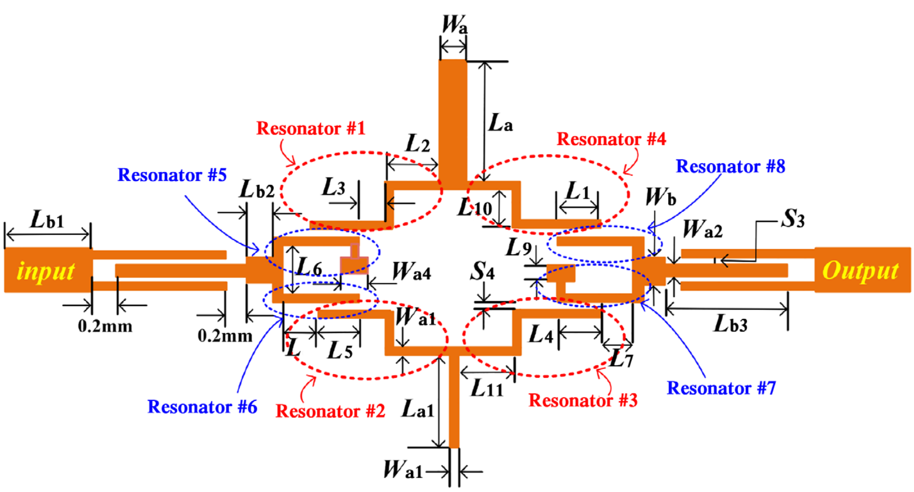

FIGURE 1 Structure of the proposed single-layer planar triband bandpass filter

$$Y = Y_1 + Y_2 + Y_3, \quad (1)$$

where,

$$Y_1 = -jZ_2\left[\frac{Z_1 - Z_2\tan\theta_1\tan\theta_2}{Z_2\tan\theta_1 + Z_1\tan\theta_2}\right], \quad (2a)$$

$$Y_2 = j\frac{\tan\theta_5}{Z_5}, \quad (2b)$$

$$Y_3 = -jZ_3\left[\frac{Z_4 - Z_3\tan\theta_3\tan\theta_4}{Z_3\tan\theta_4 + Z_4\tan\theta_3}\right]. \quad (2c)$$

The condition for resonance is when $Y = 0$. This occurs when the numerators in Equations (2a)–(2c) are equated to zero, thus:

$$Z_1 - Z_2\tan\theta_1\tan\theta_2 = 0, \quad (3a)$$

$$\tan\theta_5 = 0, \quad (3b)$$

$$Z_4 - Z_3\tan\theta_3\tan\theta_4 = 0, \quad (3c)$$

To simply the analysis, $\theta_1 = \theta_2 = \theta_x$ and $\theta_3 = \theta_4 = \theta_y$ then Equations (3a) and (3c) reduce to:

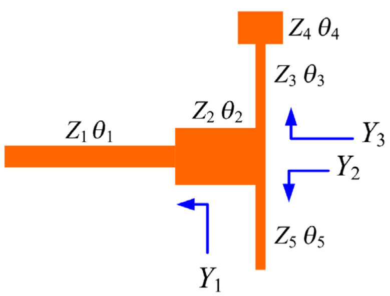

FIGURE 2 Microstrip resonator section in the proposed triband bandpass filter that is electromagnetically coupled with the input/output and T-shaped resonators

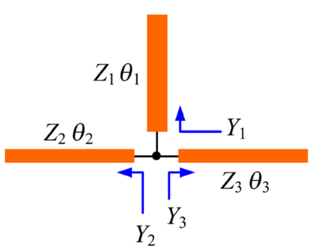

FIGURE 3 T-shaped microstrip-line resonant structure constituting the triband filter

$$1 - k_x\tan^2\theta_x = 0, \quad (4a)$$

$$1 - k_y\tan^2\theta_y = 0, \quad (4b)$$

where, impedance ratio $k_x = Z_2/Z_1$ and $k_y = Z_3/Z_4$. As the electrical length $\theta = 2\pi f/c$, from Equations (3b), (4a) and (4b) the structure generates resonance modes corresponding to:

$$\theta_{r1} = \pi, \quad (5a)$$

$$\theta_{r2} = \tan^{-1}\sqrt{1/k_x}, \quad (5b)$$

$$\theta_{r3} = \tan^{-1}\sqrt{1/k_y}, \quad (5c)$$

The T-shaped microstrip-line resonator that couples the two open-loop resonators in the triband filter is shown in isolation in Figure 3. The overall admittance of this structure is the sum of the individual admittances labeled in Figure 3 that is:

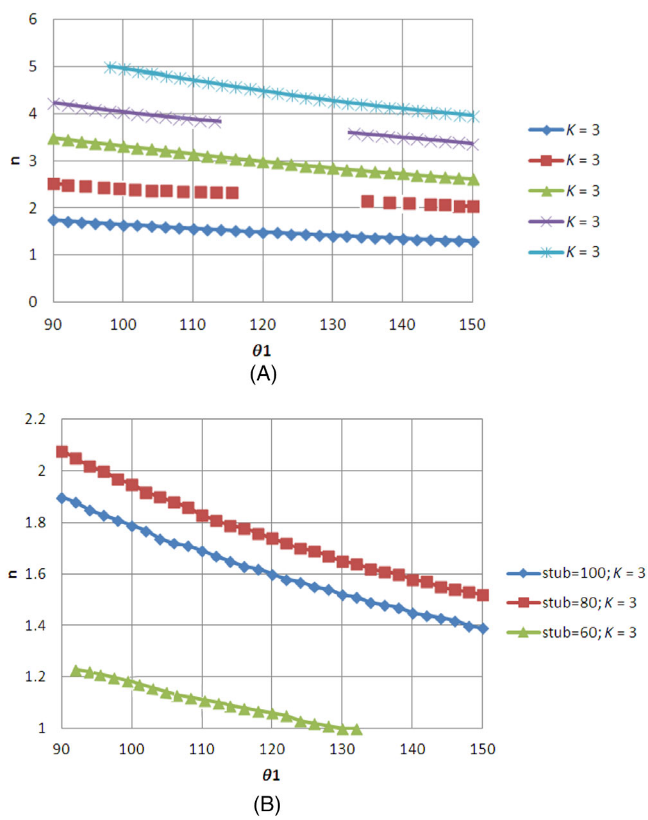

FIGURE 4 (A) Resonance frequency ratio (n) of higher order modes with respect to the fundamental frequency as a function of stub length (θ_1) in degrees and k, and (B) resonance frequency ratio as a function of stub length for different stub lengths in degrees

$$Y = Y_1 + Y_2 + Y_3, \tag{6}$$

$$\text{or } Y = j\left[\frac{Z_2Z_3\tan\theta_1 + Z_1Z_3\tan\theta_2 + Z_1Z_3\tan\theta_3}{Z_1Z_2Z_3}\right], \tag{7}$$

At resonance $Y = 0$. This condition is met when the numerator in Equation (7) is equated to zero, thus:

$$Z_2Z_3\tan\theta_1 + Z_1Z_3\tan\theta_2 + Z_1Z_3\tan\theta_3 = 0. \tag{8}$$

From Figure 1 it is evident that $Z_2 = Z_3 = Z$ and $\theta_2 = \theta_3 = \theta$. This simplifies Equation (8) to:

$$\tan(n\theta_1) + 2k_z\tan(n\theta) = 0. \tag{9}$$

where n is the ratio of resonance frequency to the fundamental frequency; and k_z is the impedance ratio Z_1/Z.

Figure 4A is based on Equation (9). It shows how the resonance frequency ratio varies with open circuit stub length (θ_1) and impedance ratio k_z. This graph confirms the modes generated by the structure can be controlled by changing stub length and the impedance ratio. Figure 4B shows how the frequency ratio is affected by the stub length for a given magnitude of impedance ration. The results show that dual mode resonance is generated by the T-shaped structure.

Figure 5 shows simplification of the open-loop resonators constituting the proposed triband filter. The input/output feedlines divide the resonators into two sections of l_1 and l_2. The total length of the resonator is $l = l_1 + l_2 = \lambda_g/2$, where λ_g is the guided wavelength at fundamental resonance.

The ABCD matrix for the upper and lower sections of the lossless circuit in Figure 5 are:

$$\begin{bmatrix} A & B \\ C & D \end{bmatrix}_{\text{upper}} = M_1M_2M_3, \tag{10a}$$

$$\begin{bmatrix} A & B \\ C & D \end{bmatrix}_{\text{lower}} = M_3M_2M_1, \tag{10b}$$

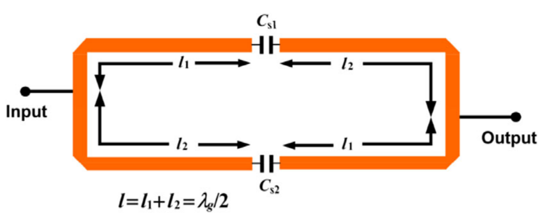

FIGURE 5 Open-loop resonators

where,

$$M_1 = \begin{bmatrix} \cos\beta l_1 & jZ_0\sin\beta l_1 \\ jY_0\sin\beta l_1 & \cos\beta l_1 \end{bmatrix}, M_2 = \begin{bmatrix} 1 & Z_c \\ 0 & 1 \end{bmatrix},$$

$$M_3 = \begin{bmatrix} \cos\beta l_2 & jZ_0\sin\beta l_2 \\ jY_0\sin\beta l_2 & \cos\beta l_2 \end{bmatrix},$$

where β is the propagation constant, $Z_c = 1/j\omega C_{s1}$ is the impedance of the gap capacitance C_{S1}, ω is the angular frequency, and $Z_o = 1/Y_o$ is the characteristic impedance of the resonator.

The Y-parameters of the upper and lower sections are obtained from Equations (10a) and (10b) and given by:

$$\begin{bmatrix} Y_{11} & Y_{12} \\ Y_{21} & Y_{22} \end{bmatrix} = \begin{bmatrix} \frac{D_j}{B_j} & \frac{B_jC_j - A_jD_j}{B_j} \\ \frac{-1}{B_j} & \frac{A_j}{B_j} \end{bmatrix}, \tag{11}$$

where j = upper or lower section. In addition, Y parameter of the whole circuit is expressed as:

$$\begin{bmatrix} Y_{11} & Y_{12} \\ Y_{21} & Y_{22} \end{bmatrix} = \begin{bmatrix} Y_{11} & Y_{12} \\ Y_{21} & Y_{22} \end{bmatrix}_{\text{upper}} + \begin{bmatrix} Y_{11} & Y_{12} \\ Y_{21} & Y_{22} \end{bmatrix}_{\text{lower}}. \tag{12}$$

The insertion-loss (S_{21}) of the circuit can then be calculated from the total Y-parameters given by:

$$S_{21} = \frac{-2Y_{21}Y_0}{(Y_{11}+Y_0)(Y_{11}+Y_0) - Y_{12}Y_{21}}. \tag{13}$$

The open-loop resonator's insertion-loss (S_{21}) can be shown to be given by:

$$S_{21} = \frac{j4\left(Z_0\sin\beta l - \frac{\cos\beta l_1\cos\beta l_2}{\omega C_{s1}}\right)Y_0}{\left[2\cos\beta l + \frac{Y_0\sin\beta l}{\omega C_{s1}} + j\left(Z_0\sin\beta l - \frac{\cos\beta l_1\cos\beta l_2}{\omega C_{s1}}\right)Y_0\right]^2 - 4}. \tag{14}$$

By letting $S_{21} = 0$ the transmission zeros can be determined, namely

$$Z_0\sin\beta l - \cos\beta l_1\cos\beta l_2/\omega C_{s1} = 0. \tag{15}$$

For a large gap between the resonators C_{s1} is negligible, so the above equation can be approximated as:

$$\cos\beta l_1 \cos\beta l_2 = 0. \tag{16}$$

Equation (16) shows the relation between the transmission zeros and the tapping positions. By substituting $\beta = 2\pi f\sqrt{\varepsilon_{\text{eff}}}/c$ in Equation (16), the transmission zeros corresponding to the tapping positions are found to be:

$$f_{\text{tz1}} = nc/4l_1\sqrt{\varepsilon_{\text{eff}}}, \tag{17a}$$

$$f_{\text{tz2}} = nc/4l_2\sqrt{\varepsilon_{\text{eff}}}, \tag{17b}$$

where $n = 1, 3, 5,...$

3 | PARAMETER ANALYSIS

A parametric study was conducted to investigate how the geometry of the filter structure influenced its triband response. This was done using ADS™ Momentum electromagnetic tool by Keysight Technologies. The filter was constructed on substrate Arlon CuClad217LX with thickness (h) of 0.794 mm, dielectric constant (ε_r) of 2.17 mm, copper conductor thickness (t) of 35 μm, and loss-tangent (tanδ) of 0.0009.

Figure 6 shows that although the coupled resonator length (L_{b3}) has no effect on the insertion-loss (IL) response, but it affects the return-loss of the three passbands. The return-loss (RL) of passbands one and three can be changed by about 47% and 29%, respectively, and RL of passband two can be changed by just 16.5%.

Figure 7 shows the performance of a triband filter as a function of resonator width (W_{a4}). The simulation results reveal compared to the RL of the second and third passbands W_{a4} significantly affects the RL of the first passband. It also affects the center frequency of the first passband (f_1) as well as the frequency of the first transmission zero (f_{tz1}). It has no effect on the center frequency of the second (f_2) and third (f_3) passbands.

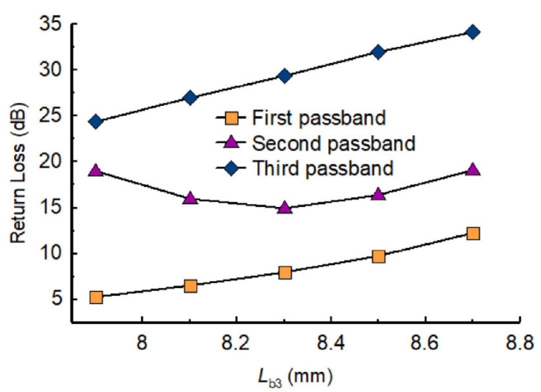

FIGURE 6 Effect on the filter's return-loss as a function of resonator length (L_{b3})

Resonator length (L_a) only affects the IL and RL of the third passband, as shown in Figure 8. It also has an influence on the center frequency of the third (f_{tz3}) and fifth (f_{tz5}) transmission zeros. The center frequency of the fifth transmission zero significantly reduces for L_a greater than 4.4 mm. These results show that we can tune (i) the transmission zeros f_{tz3} by 5% and f_{tz5} by 7%; and (ii) the center frequency by 7%.

Resonator length (L_{10}) has marginal effect on the center frequency of the filter's second passband and transmission zeros f_{tz2}, f_{tz3}, and f_{tz4}, as shown in Figure 9. However, L_{10} has a significant effect on the return-loss of all three passbands. In fact, the return-loss of the first and third passband improve with reduction in L_{10} but the converse is true for the second passband.

Figure 10 shows resonator length (L_5) has marginal effect on the center frequencies of the second and third passbands and the transmission zeros of f_{tz1} to f_{tz4}. However, L_5 affects the return-loss of the first and third passbands. Figure 11 show the resonator length (L_6) has insignificant effect the center frequencies of the filter's passbands and transmission zeros. However, it only affects the *RL* of the second passband.

Resonator length (L_9) influences the filter's first passband and the first transmission zero, as shown in Figure 12. It also significantly affects the return-loss of all three passbands. Figure 12 shows that as the length is increased the return-loss of the second and third passbands deteriorate whereas the return-loss of the first passband improves up to a length of 2.2 mm and thereafter the return-loss worsens.

Resonator length (L_8) only affects the passband of the first response. The return-loss first declines with increase in L_8 from 2.71 mm to 3 mm, and then improves for lengths larger than 3 mm, as shown in Figure 13. The also shows the center frequency of the first passband reduces almost linearly with increase in L_8 from 2.71 to 3.61 mm.

The effect of resonator length (L_3) on the filter's performance is shown in Figure 14. L_3 has marginal effect on the center frequencies of the second and third passbands and the third and fourth transmission zeros. The figure shows the return-loss of the first passband moderately declines with increase in L_3 however the passband of the second passband increases. In the case of the third passband, the return-loss first falls with increase in L_3 then rises for lengths greater than 2.16 mm.

The influence of resonator length (L_2) on the filter's response is shown in Figure 15. The results show L_2 has

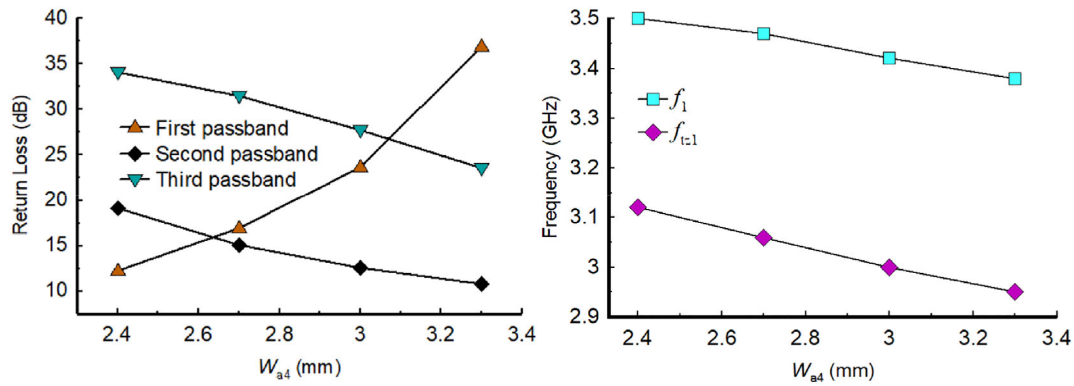

FIGURE 7 Effect on the triband filter's return-loss, center frequency and first transmission zero as a function of resonator width (W_{a4})

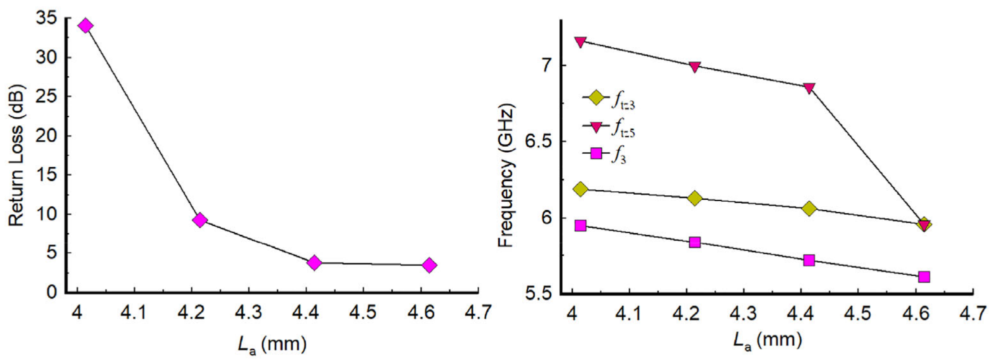

FIGURE 8 Effect of the resonator length (L_a) on the triband filter's third passband return-loss and center frequency as well as the center frequency of the third passband and fifth transmission zero

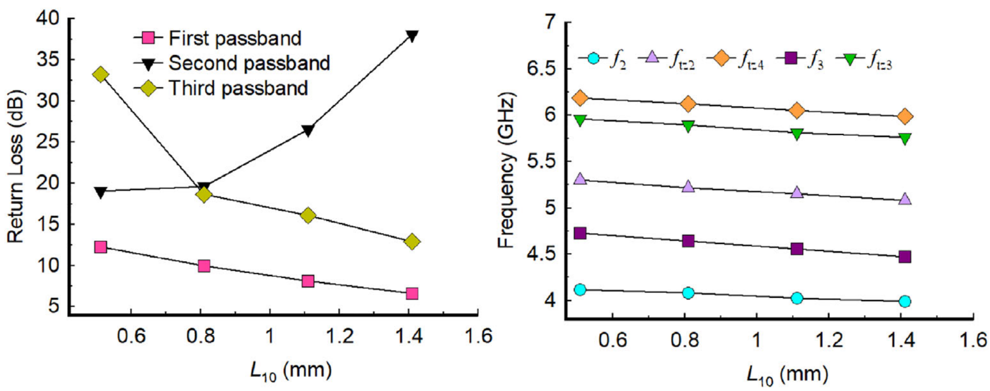

FIGURE 9 Effect on the triband filter's return-loss and center frequencies of the second and third passbands and the second, third and fourth transmission zeros as a function of resonator length (L_{10})

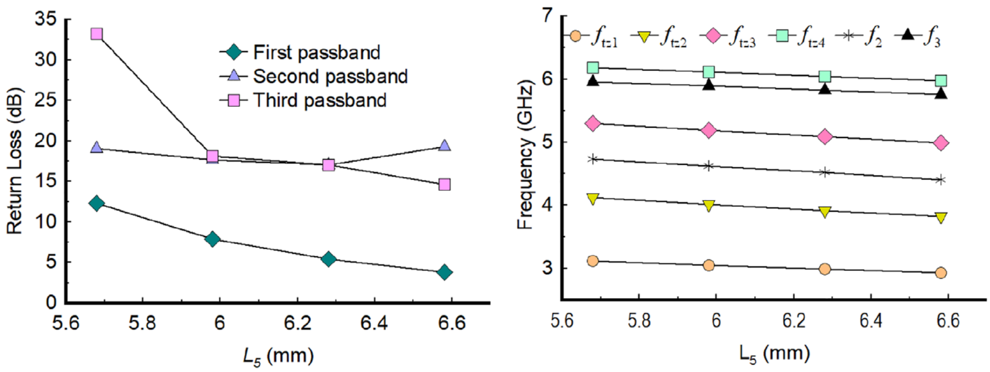

FIGURE 10 Effect on the triband filter's return-loss and center frequencies of the second and third passbands and the first, second, third and fourth transmission zeros as a function of resonator length (L_5)

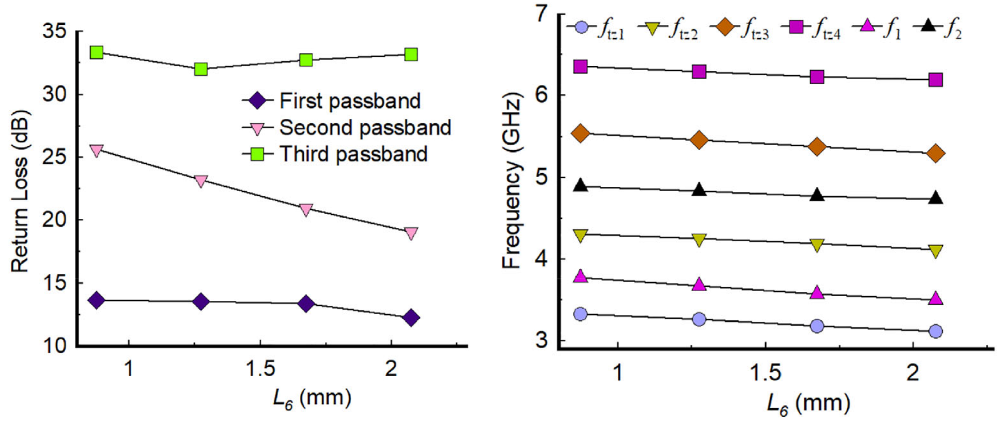

FIGURE 11 Effect on the triband filter's return-loss and center frequencies of the first and second passbands and the first, second, third and fourth transmission zeros as a function of resonator length (L_6)

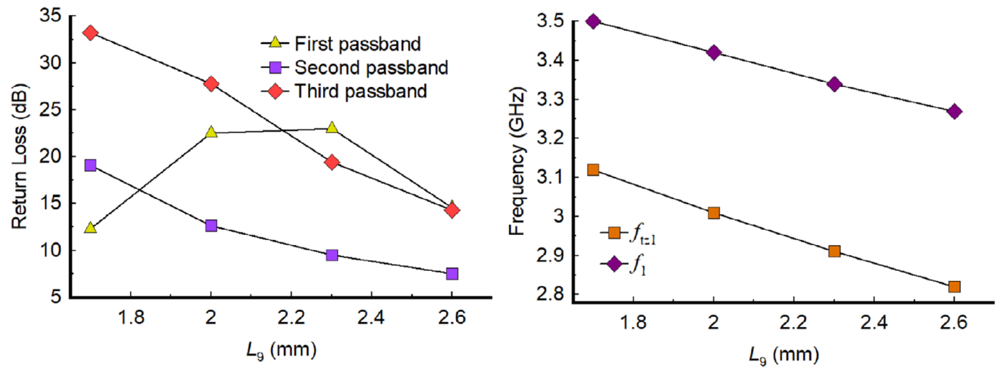

FIGURE 12 Effect on the triband filter's return-loss and center frequencies of the first passband and the first transmission zeros as a function of resonator length (L_9)

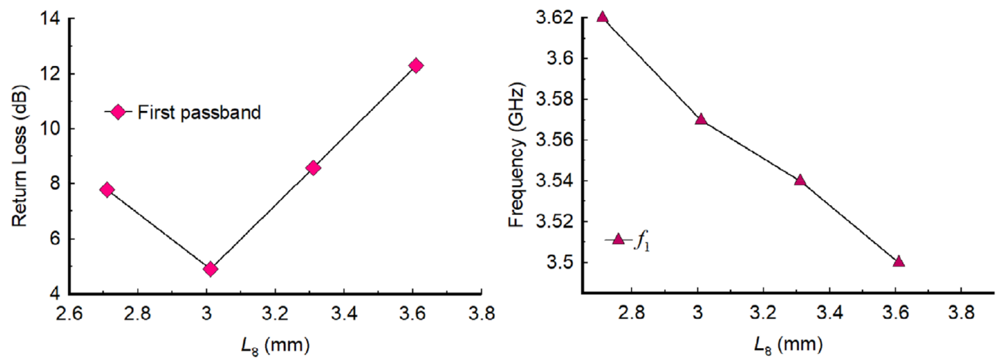

FIGURE 13 Effect on the triband filter's return-loss and center frequencies of the first passband as a function of resonator length (L_8)

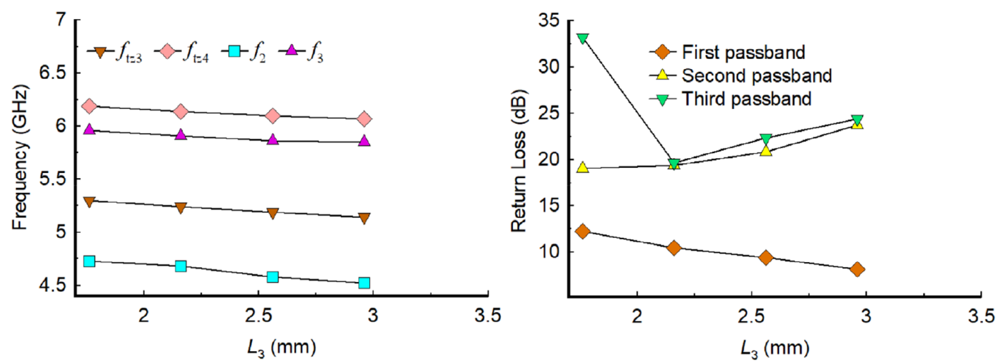

FIGURE 14 Effect on the triband filter's center frequencies of the second and third passband and third and fourth transmission zeros, and the return loss as a function of resonator length (L_3)

little effect on the transmission zeros (f_{tz2}, f_{tz3}, and f_{tz4}), center frequencies (f_2 and f_3). However, the return-loss the first and third passbands are affected significantly more than the second passband with change in L_2. In fact, the return-loss of the first and second passbands change conversely with increase in L_2.

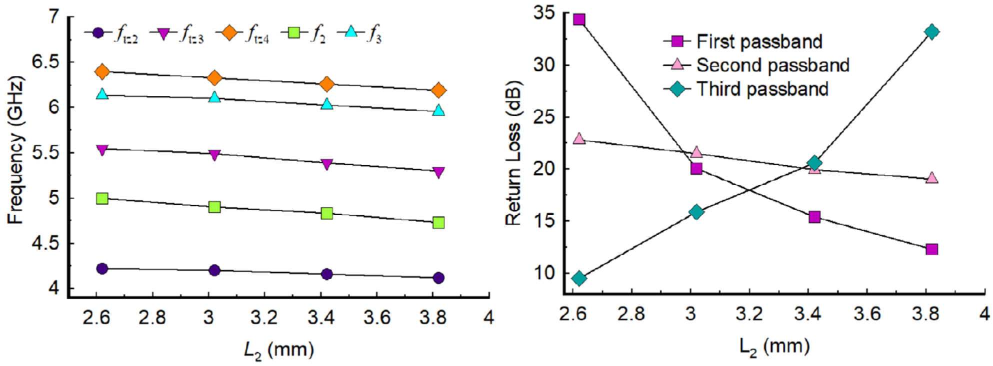

FIGURE 15 Effect on the triband filter's center frequencies of the second and third passband and second and third transmission zeros, and the return loss as a function of resonator length (L_2)

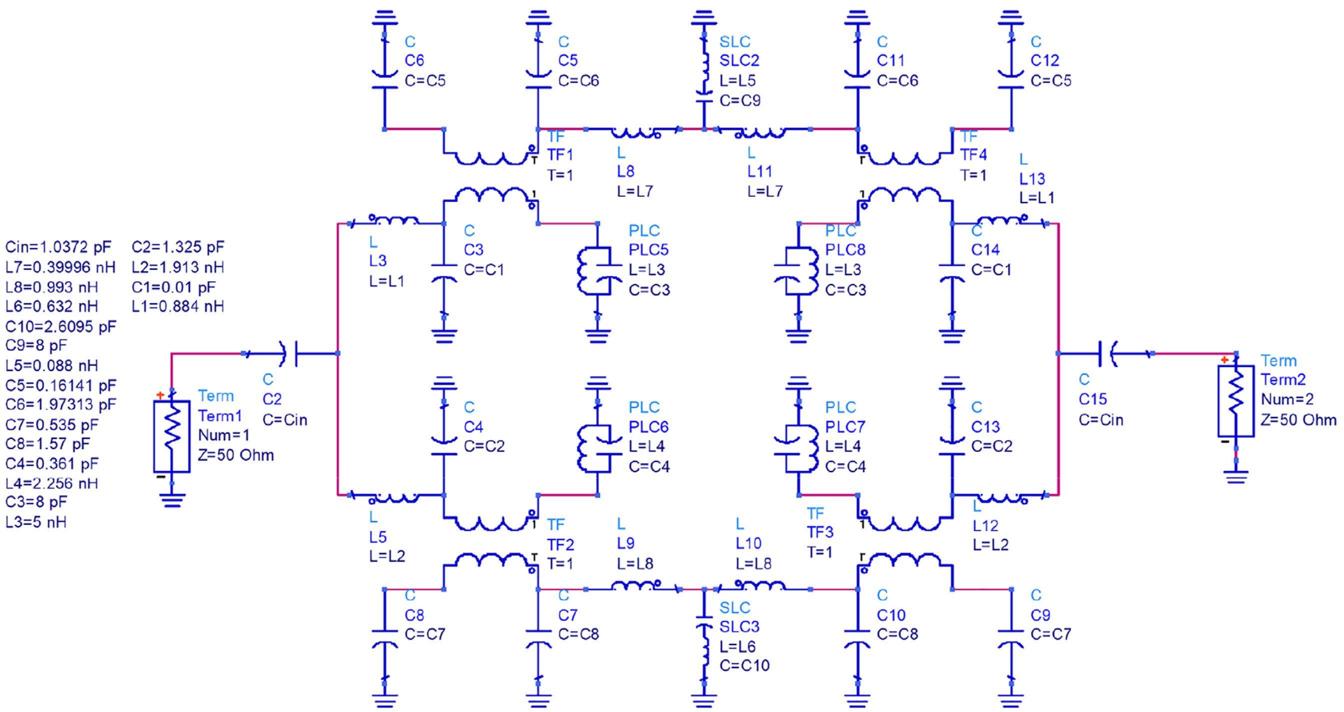

FIGURE 16 Equivalent lumped element circuit model of the proposed filter

4 | DESIGN PROCEDURE

A triband bandpass filter was designed to isolate the following bands: WiMAX (3.4–3.6 GHz), WLAN (5.15–5.85 GHz), and 4.5 GHz band which is been considered for 5G digital beamforming in dense urban areas. Design methodology of the filter is based on the information obtained in the above parametric study. This involves first establishing the dimensions of each resonator constituting the filter at the three respective passband center frequencies of interest. The length of the U-shaped open-loop resonator at the input and output ports, shown in Figure 1, are calculated using Equations (17a) and (17b) to establish the filter's outer transmission zeros. The three passbands are determined by the electrical length and impedance ratios (Z_2/Z_1 and Z_3/Z_4) of the asymmetric T-shaped structure in Figure 2 as defined by Equations (5a)–(5c). The length (L_a) of the T-shaped resonator coupling the two U-shaped open-loop resonators is determined by Equation (9). The width of the input/output ports correspond to 50 Ω. The width of the open-circuited stubs was selected for minimal impact on the passband insertion-loss. Resonator width (W_{a4}) determine the center frequency and first transmission zero (f_{tz1}). The coupled resonator length (L_{b3}) and resonator length (L_{10}) are chosen for passband return-loss better than 25 dB. Resonator width (W_{a4}) is used to fine tune the center frequency and first transmission zero (f_{tz1}). Resonator length (L_a) is used to adjust the center frequency of the third (f_{tz3}) and fifth (f_{tz5}) transmission zeros. Resonator length (L_6) can also be used to finely adjust the filter's passbands, but its affect is marginal. Resonator length (L_9) is used to adjust the filter's first passband and the first transmission zero. Resonator length (L_8) can be used to tune the passband of the first response. ADS™ was used to optimize the triband filter.

The lumped element equivalent circuit model of the filter is shown in Figure 16. The fabricated triband bandpass filter is shown in Figure 17. The optimized dimensions in millimeters of the filter are $W_a = 0.92$, $W_{a1} = 0.20$, $W_{a2} = 0.20$, $W_{b4} = 2.40$, $W_{b5} = 0.20$, $L_a = 8.03$, $L_{a1} = 8.87$, $L_{b1} = 3$, $L_{b2} = 1.04$, $L_{b3} = 8.72$, $L_1 = 5.56$, $L_2 = 3.82$, $L_3 = 1.76$, $L_4 = 2.12$, $L_5 = 5.68$, $L_6 = 2.07$, $L_7 = 3.67$, $L_8 = 3.61$, $L_9 = 1.70$, $L_{10} = 0.72$, $L_{11} = 4.76$, $S_3 = 0.20$, and $S_4 = 0.26$.

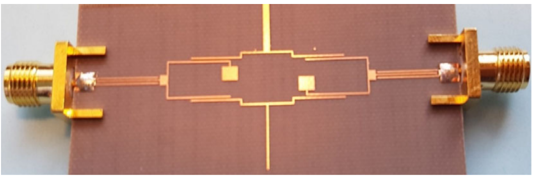

FIGURE 17 Photograph of the fabricated triband bandpass filter

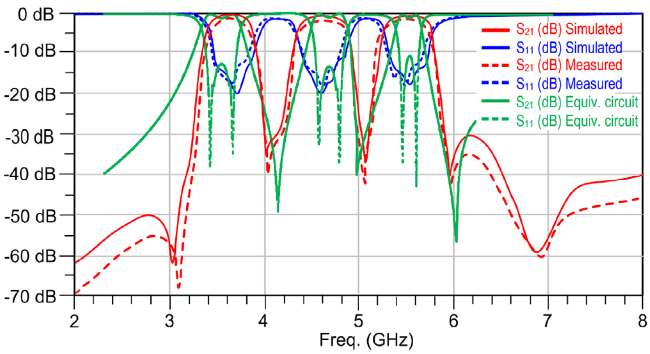

FIGURE 18 Simulated and measured insertion-loss and reflection-coefficient response of the proposed triband bandpass filter

Figure 18 shows the filter's theoretical, simulated and measured performance. The simulation was conducted using Momentum in Advanced Design System by Keysight Technologies. The triband has identical 3-dB bandwidth of 0.43 GHz located at 3.6, 4.6, and 5.5 GHz. The measured passband insertion-loss at each band is 0.78 dB and the reflection-coefficient is better than −10 dB. The isolation between the passbands is greater than 30 dB. There is excellent correlation between the simulated and measured. Although the center frequencies of the theoretical model agree with the measured results however the discrepancy in the 3-dB bandwidth of the second and third passbands are inconsistent. This is attributed to the distributed elements of the microstrip transmission lines constituting the filter circuit.

Table 1 compares the proposed triband filter with representative prior works. Compared to other triband filters the proposed design can be configured to realize passbands of equal 3-dB bandwidth. In addition, it has significantly sharper roll-off rate (>119 dB/GHz) than the previous works cited with the exception of Reference [23]. In addition, compared to the HTS bandpass filter in Reference [11] the proposed structure has a superior roll-off rate greater than 87.9 dB/GHz. Moreover, the proposed filter can be printed on a single layer of the substrate with no need for any short-circuited plated through hole. This mitigates fabrication complexity and reduces production cost. Although the size of the proposed triband filter is relatively large compared to other filters this can be remedied by fabricating the

TABLE 1 Comparison of the proposed triband filter with prior works

Ref.	No. of Tz's	Freq. bands (GHz)			3-dB FBW (%)			ξ_{ROR} (dB/GHz)			Size ($\lambda_g \times \lambda_g$)
[12]	4	7.5	12.6	18.7	1	1.6	1.4	3.8	5.4	5.3	0.19 × 0.19
[13]	3	1.57	2.48	3.5	17.1	1.8	13.7	18.5	60	46	0.14 × 0.22
[14]	4	1.56	2.45	3.5	14.3	22	9.9	108	87	113	0.15 × 0.16
[15]	3	2.5	3.7	5	16.7	14.4	13	73	42.7	24	0.31 × 0.32
[16]	2	2.3	3.4	5.2	20.8	7.7	11.1	23	37.5	24	0.19 × 0.21
[17]	3	2.5	3.6	4.5	10	12.8	8.0	49	55	27	0.26 × 0.23
[18]	6	0.85	1.57	2.4	16.8	3.5	9.6	35	80	138	0.10 × 0.09
[19]	5	7.7	11	12.1	4.63	3.4	3.1	113	56	113	1.52 × 1.52
[20]	4	1.72	4.72	7.59	30.2	34.7	7.1	16	36	20.6	0.09 × 0.51
[21]	4	3.5	5.2	8.1	7.3	2	1.1	15.4	4.2	34	0.38 × 0.28
[22]	7	1.77	2.37	3.43	7.3	2	1.1	63.9	68.1	72.5	0.32 × 0.27
[23]	6	0.40	0.94	1.72	10.4	8.3	4.5	161	129	161	0.32 × 0.32
[24]	5	1.57	2.45	3.5	4.3	9.1	1.2	107	64	53.8	0.70 × 0.48
This work	5	3.6	4.6	5.6	11.9	11.9	11.9	158	153	119	0.97 × 0.41

Note: Roll-off defined as $\xi_{ROR} = |\delta_{-20\,dB} - \delta_{-3\,dB}|/(f_{-20\,dB} - f_{-3\,dB})$, where $\delta_{-20\,dB/-3\,dB}$ are the 20 dB/3 dB attenuation points, and $f_{-20\,dB/-3\,dB}$ are the 20 dB/3 dB stopband frequencies of $|S_{11}|$.

Abbreviations: FBW, fractional bandwidth; Tz, transmission zero.

structure on a high dielectric constant substrate, as the guided wavelength inside a microstrip is inversely proportional to the square root of effective dielectric constant.

5 | CONCLUSION

The proposed triband bandpass structure, which is based on multimode stepped impedance resonator, is shown to exhibit a very sharp selectivity, equal passbands, high inter-band isolation and wide stopbands. Moreover, the filter can be printed on a single layer of substrate and requires no short circuit vias. The filter's transmission zeros can be manipulated to realize the required passband center frequency and bandwidths. The triband filter meets the need for multiband characteristics from a single device, which are in high demand for multifunctional services in the latest wireless systems.

DATA AVAILABILITY STATEMENT

Data sharing not applicable to this article as no datasets were generated or analysed during the current study.

ORCID

Bal S. Virdee https://orcid.org/0000-0001-7203-0039

REFERENCES

1. V. Crnojević-Bengin. Advances in multi-band microstrip filters. Cambridge University Press; 2015. ISBN: 9781139976763.
2. Fu S, Wu B, Chen J, Sun S-J, Liang C-H. Novel second order dual-mode dual-band filters using capacitance loaded square loop resonator. *IEEE Trans Microw Theory Tech*. 2012;60(3):477-483.
3. Kim CH, Chang K. Independently controllable dual-band bandpass filters using asymmetric stepped-impedance resonators. *IEEE Trans Microw Theory Tech*. 2011;59(12):3037-3047.
4. Zhang SB, Zhu L. Synthesis design of dual-band bandpass filters with stepped-impedance resonators. *IEEE Trans Microw Theory Tech*. 2013;61(5):1812-1819.
5. Mondal P, Mandal MK. Design of dual-band bandpass filters using stub-loaded open-loop resonators. *IEEE Trans Microw Theory Tech*. 2008;56(1):150-155.
6. Xiao J-K, Li Y, Zu X-P, Zhao W. Multi-mode multi-band bandpass filter using hexagonal patch resonator. *Int J Electron*. 2014;102(2):283-292.
7. Karimi M, Sadough SMS. Improved spectrum sensing and achieved throughput of multiband cognitive radio systems under probabilistic spectrum access. *AEU-Int J Electron C*. 2018;86:8-16.
8. Wei F, Qin P-Y, Guo J. Design of multi-band bandpass filters based on stub loaded stepped-impedance resonator with defected microstrip structure. *IET Microw Antennas Propag*. 2016;10(2):230-236.
9. Wei F, Qin P-Y, Guo J. Compact balanced dual and tri-band BPFs based on stub loaded resonators. *IEEE Microwave Wireless Compon Lett*. 2015;25(2):76-78.
10. Xu J. Compact microstrip tri-band bandpass filter using new stubs loaded stepped impedance resonator. *IEEE Microwave Wireless Compon Lett*. 2016;26(4):249-251.
11. Long Z, Tian M, Zhang T, Qiao M, Wu T, Lan Y. High temperature superconducting multimode dual-ring UWB bandpass filter. *IEEE Trans Appl Superconduct*. 2020;30(2):1-4.
12. Yan M, Wang J, Ma H. A tri-band, highly selective, bandpass FSS using cascaded multilayer loop arrays. *IEEE Trans Antennas Propag*. 2016;64(5):2046-2049.
13. Wei F, Qin P-Y, Guo J. Compact balanced dual and tri-band BPFs based on coupled complementary split-ring resonators (C-CSRR). *IEEE Microw and Wireless Compon Lett*. 2016;26(2):107-109.
14. Ai J, Zhang YH, Xu KD, Shen MK, Joines WT. Miniaturized frequency controllable band-stop filter using coupled-line stub-loaded shorted SIR for tri-band application. *IEEE Microw Wireless Comp Lett*. 2017;27(7):627-629.
15. Wang ZJ, Wang C, Kim NY. Dual−/triple-wideband microstrip bandpass filter using independent triple-mode stub-loaded resonator. *Microw Opt Technol Lett*. 2018;60(1):56-64.
16. Zhang S-F, Wang LT, Zhao SH, et al. Design of dual−/tri-band BPF with controllable band-width based on a quintuple-mode resonator. *Prog Electro Lett*. 2019;82:129-137.
17. K.-H. Wang and J.-S. Li, "Compact tri-band BPF based on embedded asymmetric T-shape stub-loaded resonators. 12th International Symposium on Antennas, Propagation and EM Theory (ISAPE), 2018, pp. 1–3.
18. Basit A, Khattak MI, Sebak AR, Qazi AB, Telba AA. Design of a compact microstrip triple independently controlled pass bands filter for GSM, GPS and WiFi applications. *IEEE Access*. 2020;8:77156-77163.
19. Zhang J, Liu Q, Zhou D, Zhang S. Single- and triple-band bandpass filters using novel perturbed isosceles right-angled triangular SIW cavities. *IET Microwaves Antennas Propag*. 2021;15:241-252.
20. Al-Yasir YIA, Tu Y, Bakr MS, et al. Design of multi-standard single/tri/quint-wideband asymmetric step impedance resonator filters with adjustable transmission zeros. *IET Microwaves Antennas Propag*. 2019;13(10):1637-1645.
21. Karimi G, Rostaie P, Sabaghi F. New approach design of compact tri-band microstrip bandpass filter based on combined stepped-impedance resonator and triangular patches. *Microw Opt Technol Lett*. 2020;26:3170-3174.
22. Zhu L, Guan Y, Zheng B, Cheng Z. A high selectivity tri-band BPF using π-type structure loaded with λ/4 open stub and hybrid SIR. *Microw Opt Technol Lett*. 2022;64:905-910.
23. Killamsetty VK, Mukherjee B. Compact triple band bandpass filters design using mixed coupled resonators. *AEU-Int J Electron Commun*. 2019;107:49-56.
24. Chen L, Peng JY, Wang M, Zhang TT, Wei F. Compact balanced tri-band bandpass filter based on stub loaded resonator with high selectivity. *Int J RF Microwave Comput-Aided Eng*. 2021;31(12):1-8.

How to cite this article: Riaz M, Virdee BS, Mariyanayagam D, Salekzamankhani S, Benetatos H, Lubangakene I. Sharp roll-off triband microstrip bandpass filter with wide stopband for multiband wireless communication systems. *Int J RF Microw Comput Aided Eng*. 2022;e23438. doi:10.1002/mmce.23438